JACS
JOURNAL OF THE AMERICAN CHEMICAL SOCIETY
Article
pubs.acs.org/JACS

Mixed Close-Packed Cobalt Molybdenum Nitrides as Non-noble Metal Electrocatalysts for the Hydrogen Evolution Reaction

Bingfei Cao,[†,‡] Gabriel M. Veith,[§] Joerg C. Neuefeind,[∥] Radoslav R. Adzic,[‡] and Peter G. Khalifah*[,†,‡]

[†]Chemistry Department, Stony Brook University, Stony Brook, New York 11794, United States
[‡]Chemistry Department, Brookhaven National Laboratory, Upton, New York 11793, United States
[§]Material Science and Technology Division and [∥]Chemical and Engineering Materials Division, Oak Ridge National Laboratory, Oak Ridge, Tennessee 37831, United States

Supporting Information

ABSTRACT: A two-step solid-state reaction for preparing cobalt molybdenum nitride with a nanoscale morphology has been used to produce a highly active and stable electrocatalyst for the hydrogen evolution reaction (HER) under acidic conditions that achieves an *i*R-corrected current density of 10 mA cm^{-2} at −0.20 V vs RHE at low catalyst loadings of 0.24 mg/cm^2 in rotating disk experiments under a H_2 atmosphere. Neutron powder diffraction and pair distribution function (PDF) studies have been used to overcome the insensitivity of X-ray diffraction data to different transition-metal nitride structural polytypes and show that this cobalt molybdenum nitride crystallizes in space group $P6_3/mmc$ with lattice parameters of a = 2.85176(2) Å and c = 10.9862(3) Å and a formula of $Co_{0.6}Mo_{1.4}N_2$. This space group results from the four-layered stacking sequence of a mixed close-packed structure with alternating layers of transition metals in octahedral and trigonal prismatic coordination and is a structure type for which HER activity has not previously been reported. Based on the accurate bond distances obtained from time-of-flight neutron diffraction data, it is determined that the octahedral sites contain a mixture of divalent Co and trivalent Mo, while the trigonal prismatic sites contain Mo in a higher oxidation state. X-ray photoelectron spectroscopy (XPS) studies confirm that at the sample surface nitrogen is present and N−H moieties are abundant.

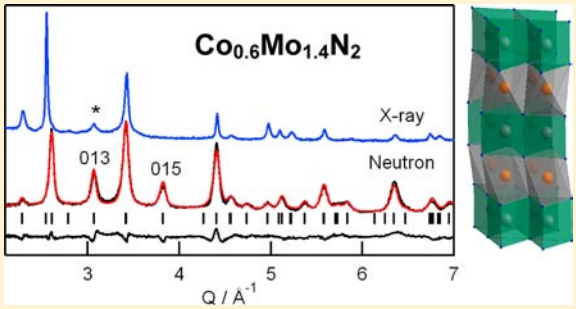

INTRODUCTION

The hydrogen evolution reaction (HER) is a central reaction in the renewable production of hydrogen fuel from water, regardless of whether this process is driven directly (solar fuel production using photons harvested by semiconductors or molecular dyes) or indirectly (electrolysis of water powered by photovoltaics).[1,2] Hydrogen produced in this manner is more easily stored and transported than electricity generated through competing photovoltaic (PV) technologies, though the overall efficiency of hydrogen production is invariably lower than that of simply generating electricity due to the energy barriers of the reactions required to produce molecular products.[3] Efficient solar energy utilization therefore requires efficient catalysts. Unfortunately, the best current HER catalysts incorporate noble metals such as Pt, whose terrestrial scarcity and high cost limit the viability of renewable H_2 production.[4]

These limitations have motivated extensive efforts to design and develop non-noble metal HER electrocatalysts which are stable under acidic environments, unlike the known classes of Ni-based HER catalysts which are only stable under alkali conditions.[5] Notable recent progress has been made in the past decade in developing acid-stable HER catalysts, resulting in the discovery of excellent HER activity for MoS_2, Mo_2C, MoB, Ni−Mo, Ni−Mo−N, and Ni_2P, which all contain Mo and/or Ni (Table S1, Supporting Information).[5−12] A good framework for understanding the influence of crystal structure on the HER activity of these compounds does not yet exist. Although methods for tuning the energy levels and catalytic activity of metallic alloys are known,[13] it is less clear how the simple binary structures of MoS_2, Mo_2C, and MoB can be tuned to optimize their activity. The bimetallic Ni−Mo−N catalyst may be more amenable to optimization, though catalytically active samples were found to contain a mixture of an ionic rock salt phase (γ-Mo_2N-type) and a Ni_2Mo_3N (Mo_3Al_2C-type) phase in which Mo is expected to be metallic in nature (valence near zero), and it has not yet been established which phase is responsible for the observed HER activity.[9]

Transition-metal nitrides are generally promising for electrocatalysis applications, as they can have both low electrical resistance and good corrosion resistance.[14] It has previously been reported that δ-MoN exhibits measurable HER activity in acidic solution, though this activity is far less than that of Ni−Mo−N and the exact nature of the δ-MoN structural polytype was not determined.[9] We were therefore motivated to investigate the electrocatalytic activity of more complex ternary

Received: August 5, 2013
Published: October 31, 2013

   dx.doi.org/10.1021/ja4081056 | J. Am. Chem. Soc. 2013, 135, 19186−19192

molybdenum nitrides in which the valence and electronic states of Mo can be more readily tuned than in binary molybdenum nitrides.

In this study, the HER activity of a nanostructured ternary cobalt molybdenum nitride produced using a low temperature synthesis route has been characterized. Neutron diffraction studies indicate that this compound has a complex layered structure that cannot be effectively resolved in X-ray diffraction experiments. This compound is demonstrated to have excellent activity toward HER despite belonging to a layered structural family for which HER activity has not previously been reported.

EXPERIMENTAL SECTION

An oxide precursor $CoMoO_4$ was prepared by dropwise addition of 20 mL (0.165 M) aqueous $CoCl_2$ (Alfa Aesar, 99.7%) into a 10 mL (0.33 M) solution of Na_2MoO_4 (Alfa Aesar). The resulting purple suspension was stirred for 1 h, filtered, washed, and dried at 120 °C overnight. Co_3Mo_3N was synthesized by annealing $CoMoO_4$ at 750 °C (5 °C/min heating rate) for 12 h under flowing ammonia (50 mL/min) inside a fused quartz tube. $CoMoN_2$ was obtained by a previously reported procedure of treating Co_3Mo_3N in NH_3 (150 cm^3/min) for 1 h at 400 °C.[15] δ-MoN was produced by treating $MoCl_5$ (Alfa Aesar, 99.6%) at 600 °C in NH_3 (150 cm^3/min) for 3 h, and this sample is described in the text as δ-MoN based on the hexagonal unit cell seen in X-ray diffraction experiments. The precise δ polytype (δ_1, δ_2, δ_3) cannot be resolved in these experiments, though the δ_1 polytype has been reported to form under these conditions.[16]

Laboratory X-ray powder diffraction patterns were obtained from a D8 Advance X-ray diffractometer (Bruker, AXS) with Bragg–Brentano geometry using Cu Kα radiation. Scans were collected with a fixed divergence slit width of 0.6°, a 2θ range of 7 to 120°, a collection time of 1.5 s per step, a diffraction radius of 300 mm, and a 192 channel LynxEye position sensitive detector. Time-of-flight (TOF) neutron diffraction measurements were performed on the nanoscale-ordered materials diffractometer (NOMAD) at the Spallation Neutron Source (SNS), Oak Ridge National Laboratory. Approximately 100 mg of powder were loaded into a 2 mm diameter capillary, with data acquisition time of 100 min per sample for a total proton charge of 5.4 × 10^{12}. Data processing of both pair distribution function (PDF) and Bragg diffraction data was done using custom beamline-specific software coded in IDL. Synchrotron diffraction data were collected at the high resolution beamline 11-BM at the Advanced Photon Source (APS) of Argonne National Laboratory using a 0.8 mm diameter Kapton capillary with λ = 0.413832 Å. The TOPAS software package (Version 4.2, Bruker AXS) was used for Le Bail and Rietveld refinements of data.

Scanning electron microscopy (SEM) analysis was carried out on a JEOL 7600F high-resolution microscope with capabilities for energy-dispersive X-ray spectroscopy (EDX). Transmission electron microscopy (TEM) was performed on a JEOL 1400 microscope operated at an accelerating voltage of 120 kV. Thermogravimetric analysis (TGA) was done on a Q5000IR system (TA Instruments). TGA scans were run under flowing O_2 (25 mL/min) with ramp rates of 1 °C/min and holds at 500 °C for 10 h and then at 600 °C for 5 h.

A PHI 3056 X-ray photoelectron spectroscopy (XPS) spectrometer with an Al source in a 2 × 10^{-10} Torr vacuum chamber was used to characterize sample surfaces. The instrument was calibrated before use with Au and Ag foils. Samples were pressed into In foil (Alfa Aesar), and the foil was attached to the sample holder using carbon tape. High-resolution scans were taken with a 5.85 eV pass energy, 0.05 eV energy step, and with 100 repeats to reduce instrument noise. Charging effects were compensated by shifting binding energies based on the adventitious C 1s peak (284.8 eV). Reference MoO_2 (Alfa Aesar, 99.95%) and MoO_3 (Alfa Aesar - Puratronic) powders were used to determine the Mo $3d_{5/2}$/Mo $3d_{3/2}$ ratio for the instrument. Peak fits and atomic surface concentration analyses were performed using PHI Multipack software.

Catalyst inks for electrochemical testing were prepared by adding a mixture of 2 mg of sample (Co, δ-MoN or nominal $CoMoN_2$) and 2 mg of carbon black (Vulcan XC72) to a solution of 500 μL of Milli-Q ultrapure deionized water (18.2 MΩ), 500 μL of isopropyl alcohol (70% v/v, Aldrich), and 50 μL of Nafion-117 (5% in a mixture of lower aliphatic alcohols and water, Aldrich) and then sonicating for 30 min to disperse the catalysts in the ink. Afterward, 25 μL of fresh catalyst ink was dropped onto a glassy carbon electrode (0.196 cm^2 geometrical area, Pine Research Instrument) and dried at room temperature. The loading was 0.24 mg/cm^2 for nitride samples and 0.023 mg/cm^2 for Pt. Electrochemical measurements were conducted in a three-electrode conventional glass cell with an electrolyte solution of 0.1 M $HClO_4$, an Ag/AgCl reference electrode, and a Pt counter electrode (separated from the electrolyte by a glass frit). [***Caution!*** *Evaporation can lead to the build-up of perchlorate deposits in hoods that can explode when agitated.*] All potentials are given with respect to the reversible hydrogen electrode (RHE). HER measurements on a rotating disk electrode (RDE) were collected in H_2-saturated solutions sweeping from +0.2 to −0.5 V vs. RHE with a scan rate of 5 mV/s and a rotation speed of 1600 rpm using a Volta PGZ402 potentiostat (VoltaLab 80, Radiometer Analytical). Long-term durability tests were performed by cyclic voltammetry (CV) sweeps at 100 mV/s from +0.2 to −0.3 V vs RHE for 3000 cycles.

RESULTS AND DISCUSSION

Catalyst Synthesis, Structure, And Composition. We hypothesized that doping MoN with Co would be an effective method of tuning its properties and potentially enhancing HER activity beyond the relatively low intrinsic activity of MoN. Such a strategy was recently employed to enhance the oxygen reduction reaction (ORR) activity of Mo_2N by the substitution of CoO into its rock salt structure.[17] The direct ammonolysis of $CoMoO_4$ at temperatures between 600 and 650 °C was found to produce a hexagonal nitride of nominal formula $CoMoN_2$, but the reaction product also contained large amounts of impurity phases like cobalt metal, rock salt type Mo_2N analogues, and cubic Co_3Mo_3N. Higher temperature reactions were found to produce phase-pure Co_3Mo_3N with a lattice parameter of a = 11.0383(2) Å that we have tested and found to show weak catalytic activity for HER reaction (Figure S1, Supporting Information). The low fraction of nitrogen in Co_3Mo_3N suggests that Co and Mo are nearly metallic (a result confirmed by prior XPS studies[18]) and that the reaction conditions are too reducing.

Although the direct synthesis of $CoMoN_2$ from a $CoMoO_4$ precursor phase was found to be ineffective, Co_3Mo_3N can serve as a very effective precursor for the rapid synthesis of $CoMoN_2$ at low temperatures.[15] Our best results were obtained by treating Co_3Mo_3N under flowing NH_3 at 400 °C for 1 h, which produced $CoMoN_2$ with Co metal as the only observable impurity phase; reactions carried out at higher temperatures or for longer times exhibited increased impurity contents. A two-step ammonolysis reaction (first making Co_3Mo_3N as a precursor) was therefore used to produce bulk $CoMoN_2$ for structural and catalytic characterization.

Powder X-ray diffraction studies on $CoMoN_2$ suggest that it is isostructural with δ-MoN (Figure 1a),[16] with a = 2.85 Å, c = 2.75 Å, and space group symmetry $P\bar{6}m2$ (#187). However, it should be noted that X-ray diffraction is dominated by scattering from Mo and Co atoms and is very insensitive to the contributions of N atoms. This is particularly problematic in the case of three MoN polytypes (δ_1, δ_2, δ_3) which all contain the same arrangement of Mo atoms and differ only in the location of N atoms. These polytypes can all be indexed based on the simple WC-type lattice of δ-MoN when diffraction peaks

dx.doi.org/10.1021/ja4081056 | J. Am. Chem. Soc. 2013, 135, 19186–19192

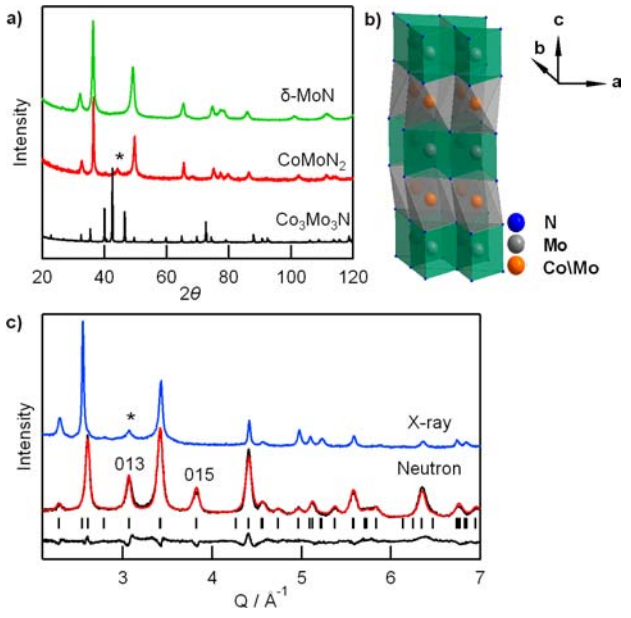

Figure 1. (a) Lab X-ray powder diffraction patterns of Co_3Mo_3N, $CoMoN_2$, and δ-MoN. Asterisk marks the impurity peak of cobalt metal. (b) Four-layered crystal structure of $CoMoN_2$. (c) Rietveld refinements of neutron diffraction for $CoMoN_2$ showing observed data (black line), calculated pattern (red line) and difference curve (bottom line). Lab X-ray diffraction data (blue line) in same Q ($= 2\pi/d$) range between 2 and 7 $Å^{-1}$ do not clearly show superstructure peaks such as the 013 and 015 reflections which are intense in neutron diffraction data.

are broad (as is the case for $CoMoN_2$) and XRD superstructure peaks are not resolvable. This occurs since only weakly scattering N atoms contribute intensity to the reflections of the superstructure peaks of δ_2-MoN ($1 \times 1 \times 2$ superstructure) and δ_3-MoN ($2 \times 2 \times 2$ superstructure),[16] where the ratio of the a- and c-lattice parameters relative to the simpler δ_1-MoN sublattice are specified. Based on prior structural data, all three molybdenum nitride structures can be described as having close packed layers of N atoms, with Mo atoms found in the voids between nitrogen layers. The coordination environment of the Mo ions is in either trigonal prismatic or octahedral, depending on whether successive nitrogen layers have the same lateral coordinates (i.e., AA) or are offset (i.e., AB).[16] Intriguingly, enhancement of the MoS_2 HER activity was recently achieved by converting the Mo environment from trigonal prismatic (2H polytype) to octahedral (1T polytype) by Li-intercalation.[12]

In order to overcome the sensitivity limitations of X-rays, neutron diffraction experiments were carried out to resolve the structure of $CoMoN_2$ since the scattering length of N (9.36 fm), Mo (6.72 fm), and Co (2.49 fm) are significantly different, giving excellent sensitivity to all species. Indexing of neutron diffraction data indicates that $CoMoN_2$ crystallizes in a $1 \times 1 \times 4$ supercell (a ~2.85 Å, c ~11.01 Å) of δ_1-MoN. Different crystal structures previously reported for transition metal nitrides were tested via Rietveld refinement, and it was found that only the $Li_{0.67}NbS_2$ structure type with $P6_3/mmc$ (#194) space group symmetry effectively described the $CoMoN_2$ structure (Figure 1c and Figures S2–S4, Supporting Information), as described in more detail in the Supporting Information. In this structure, N ions are found in close packed layers with a repeating AABB stacking sequence while all transition metal ions are found between the N layers at the coordinates directly above/below the unoccupied C layer positions of nitrogens. This leads to alternating layers of trigonal prismatic and octahedral coordination for the transition metals (Figure 1b).

Structural analogies to compounds such as $Fe_{0.8}Mo_{1.2}N_2$ suggest that Mo prefers the trigonal prismatic site (2a Wykoff position), while Co prefers the octahedral site (2b Wykoff position).[19] Although synthesis reactions were initiated with equimolar amounts of Co and Mo, and though there were no indications of the loss of Co through volatilization during the reactions, the presence of impurity peaks in the reaction product assigned to Co metal suggests that the cobalt molybdenum nitride phase is Mo-rich. The final crystallographic refinement was therefore carried out with a Co/Mo mixture on the octahedral site. No evidence was found for nonstoichiometry on the trigonal prismatic Mo site or the nitrogen site during refinement. The cobalt molybdenum nitride was found to have the stoichiometry $Co_{0.6}Mo_{1.4}N_2$. This formula is consistent with the weight fraction of Co metal (~20%) present as a second phase obtained from Rietveld refinements of X-ray diffraction data, though it should be noted that this phase fraction determination is not precise due the broad Co diffraction peaks (Tables S2–S6, Supporting Information).

The stoichiometry of the nominal $CoMoN_2$ sample can also be indirectly determined by thermogravimetric analysis. Black $CoMoN_2$ was completely oxidized to purple $CoMoO_4$ by heating the nitride in an oxygen atmosphere, as judged by powder X-ray diffraction (Figure S5, Supporting Information). The observed weight gain of $CoMoN_2$ during oxidation is 24.55 wt %, which is a little smaller than the theoretical weight gain of 25.16 wt % for the $CoMoN_2$ sample ($Co_{0.6}Mo_{1.4}N_2$ with the balance of Co present as Co metal). The smaller mass gain than expected during oxidation is attributed to the presence of a small amount of oxygen (0.61 wt %, 1.54 mol %) in the sample, which might be residing on the surface of the Co metal phase rather than being found in the $Co_{0.6}Mo_{1.4}N_2$ nitride phase. Residual oxygen is also observed in SEM-EDX analysis (Figure S6, Supporting Information) and XPS data (Table S7, Supporting Information). The active material composition of $Co_{0.6}Mo_{1.4}N_2$ is therefore supported by TGA data.

Additional insights into the crystal structure of $Co_{0.6}Mo_{1.4}N_2$ have been obtained through "small box" fitting of the neutron pair distribution function (PDF) data, shown in Figure 2. It can

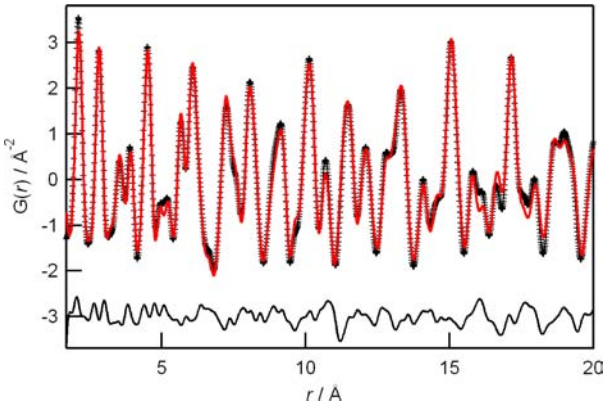

Figure 2. Neutron PDF fit from r = 1.7–20 Å for a two-phase nominal $CoMoN_2$ sample with a $1 \times 1 \times 4$ WC-superstructure phase with $P6_3/mmc$ symmetry and impurity Co metal ($Fm\bar{3}m$, #225, a = 3.56 Å).

dx.doi.org/10.1021/ja4081056 | J. Am. Chem. Soc. 2013, 135, 19186–19192

be seen that this structural model gives an excellent fit to the observed local structure over the length scale of 1.7−20 Å, suggesting that the average structure provides a very complete description of this compound even on the atomic scale. This indicates that amorphous phases are not present, as even glasses will give well-defined peaks in PDF spectra. As such, it is expected that the local environments of Co and Mo in the octahedral layer are indistinguishable, and that both ions are found at the same crystallographic position without clustering or ordering of ions within this layer. In contrast, the simple WC or NiAs structural models cannot effectively fit the PDF data (Figure S3, Supporting Information), confirming the presence of multiple Mo coordination environments, and highlighting the importance of the superstructure despite its visual absence in laboratory powder X-ray diffraction data.

Insights into particle size and morphology were obtained from electron microscopy studies (Figure 3). It can be seen in

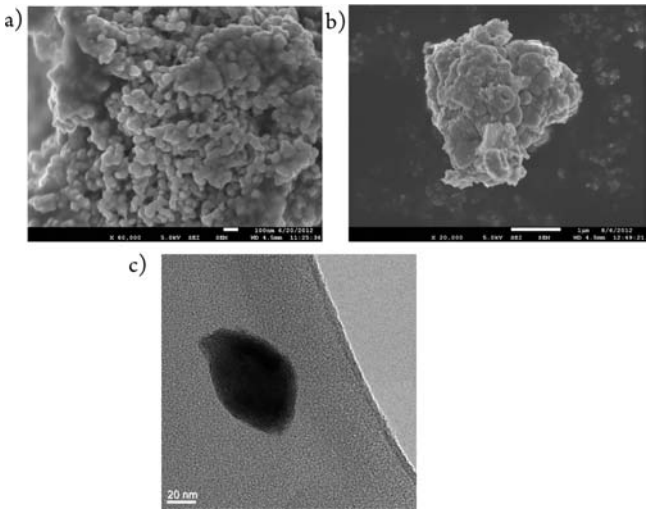

Figure 3. SEM images of (a) $Co_{0.6}Mo_{1.4}N_2$ prepared at 400 °C (scale bar: 100 nm); (b) δ-MoN synthesized at 600 °C (scale bar: 1 μm); TEM image of (c) single crystallite of $Co_{0.6}Mo_{1.4}N_2$ (scale bar: 20 nm).

SEM images that the primary particle size of $Co_{0.6}Mo_{1.4}N_2$ has nanoscale dimensions (<100 nm), and these primary particles are aggregated into larger secondary particles which can be more than a micrometer across. The secondary particle size is comparable with that of the Co_3Mo_3N precursor used in the synthesis. The primary particles of δ-MoN were substantially larger, suggesting that Co plays a role in minimizing the $Co_{0.6}Mo_{1.4}N_2$ particle size. TEM studies are able to resolve isolated crystallites of $Co_{0.6}Mo_{1.4}N_2$, and show that primary particles are typically obtained with a maximum dimension of ~80 nm but without well-defined facets.

HER Activity of Nitride Catalysts. The characterization of ternary $Co_{0.6}Mo_{1.4}N_2$ for HER activity is of particular interest given the high activity for chemical analogues such as MoS_2[6,7,12] and Ni−Mo−N nanosheets.[9] Typical polarization curves of $Co_{0.6}Mo_{1.4}N_2$ in acidic media (0.1 M $HClO_4$) under H_2 atmosphere measured in a RDE configuration are shown in Figure 4a, and it can be seen that large currents are achieved at modest overpotentials (~0.2 V), indicating excellent catalytic activity in samples prepared using a Co_3Mo_3N precursor. Data are also shown for Co metal and δ-MoN which were produced by nitridation to simulate the plausible binary reaction

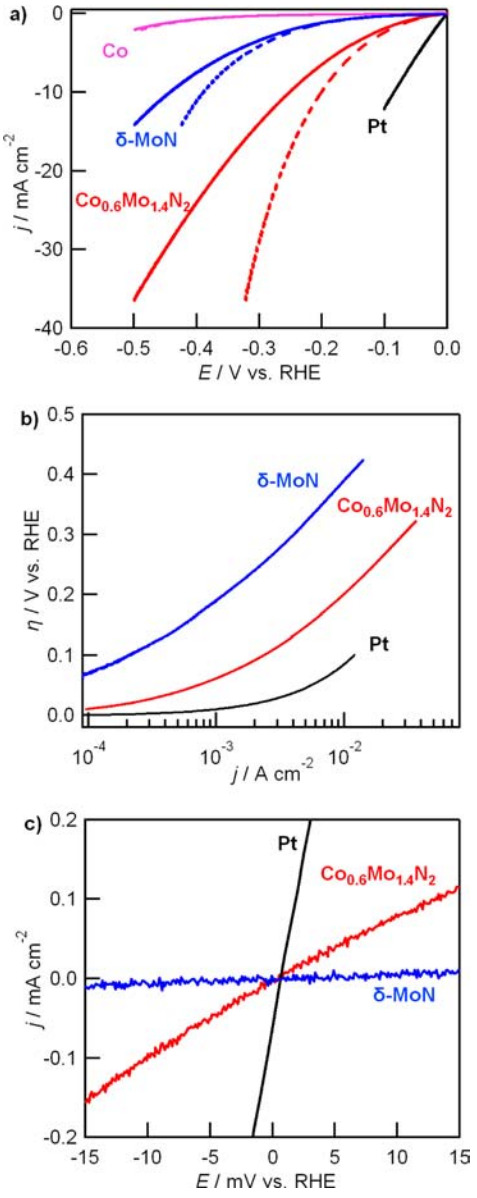

Figure 4. (a) Polarization curves of Co, δ-MoN, $Co_{0.6}Mo_{1.4}N_2$ and Pt in H_2-saturated 0.1 M $HClO_4$ with (dashed line) and without (solid line) *iR* correction. Corresponding Tafel plots (b) and current densities (c) at low overpotentials after *iR* correction.

byproducts. The activity of $Co_{0.6}Mo_{1.4}N_2$ is far higher than the binary phases which are stable under reaction conditions, strongly suggesting that $Co_{0.6}Mo_{1.4}N_2$ is the active phase for HER.

The as-measured $Co_{0.6}Mo_{1.4}N_2$ reaction currents do not directly reflect the intrinsic sample behavior due to the effects of Ohmic resistance, which was determined to be approximately 25 Ω by electrochemical impedance spectroscopy (EIS). An *iR* correction was therefore applied to the initial data, and this corrected data (dashed line, Figure 4a) was used for further analysis. A catalytic current of 10 mA/cm^2 is achieved at a potential of −0.20 V vs RHE, with this overpotential only about 0.1 V larger than needed for a Pt/C catalyst system tested under identical conditions. Although the $Co_{0.6}Mo_{1.4}N_2$ samples prepared from Co_3Mo_3N have a reasonable electronic conductivity and show good activity even in the absence of additives, the catalytic current is approximately halved when a

dx.doi.org/10.1021/ja4081056 | J. Am. Chem. Soc. 2013, 135, 19186−19192

conductive additive (carbon black) is omitted from the catalyst ink (Figure S7, Supporting Information). Another factor potentially limiting the measured HER activity is the bubbles of gaseous hydrogen evolved during the reaction. However, measurements carried out using carbon paper with good porosity and a low resistance (3.5 Ω by EIS) in place of a RDE show a lower HER activity (Figure S8, Supporting Information). This indicates that mass diffusion is limiting electrocatalytic activity in the absence of electrode rotation, as might be expected for a highly active catalyst.

The *i*R-corrected activity of $Co_{0.6}Mo_{1.4}N_2$ is rescaled and shown in the form of a Tafel plot together with the data on δ-MoN and Pt (Figure 4b), which can be used to better understand the relative performance of these systems. The simpler binary system δ-MoN requires a large overpotential (~0.3 V) before substantial catalytic currents of 5 mA/cm^2 are obtained. The lower activity of δ-MoN is reflected in the low exchange current density, j_0, of 1.5×10^{-5} A/cm^2 is found from linear fits to the low-overpotential region (Figure 4c) where the Butler−Volmer relationship further simplifies to $j = j_0 n(F/RT)\eta$ with n assumed to be 1.[20] The δ-MoN exchange current is far less than the $j_0 = 2.2 \times 10^{-3}$ A/cm^2 obtained from Pt in the linear regime. In contrast, the $Co_{0.6}Mo_{1.4}N_2$ exchange current of $j_0 = 2.3 \times 10^{-4}$ A/cm^2, which is within a single order of magnitude of the Pt activity, illustrates the high catalytic activity of this system. This exchange current density compares favorably with other Mo-based catalysts (Table S1, Supporting Information). A simple analysis of the Tafel slope of $Co_{0.6}Mo_{1.4}N_2$ is not possible as the logarithm of current density does not increase linearly with overpotential, signifying that the current is strongly influenced by back-reaction rates at low overpotentials, mass-transport at high overpotentials,[8] and/or that evolved hydrogen gas is limiting the available surface area and reaction rate at higher current densities. A robust mechanistic analysis will require more crystalline films, which will be the subject of future investigations.

The faradaic yield of H_2 production by $Co_{0.6}Mo_{1.4}N_2$ after delivery of 30 Coulombs of charge was determined to be essentially stoichiometric (>90%) by galvanostatic electrolysis, as detailed in the Supporting Information. The stability of $Co_{0.6}Mo_{1.4}N_2$ during hydrogen production is excellent, as illustrated in Figure S9 (Supporting Information). The activity of the catalyst slightly changes over the first 50 cycles between +0.2 and −0.3 V vs RHE, but remains unchanged afterward over the test period of 3000 cycles in 0.1 M $HClO_4$. This suggests that there is an initial conditioning of the catalyst through a reductive process which contributes extra current at low overpotentials. After conditioning, steady currents can be achieved. In addition to being active for HER under acidic conditions, $Co_{0.6}Mo_{1.4}N_2$ system also exhibits activity for the HER under alkaline conditions (Figure S10, Supporting Information) though with less activity (shifts to voltages ~0.1 V more negative).

In both acidic and alkaline environments, the activity of ternary $Co_{0.6}Mo_{1.4}N_2$ is very much improved over that of binary δ-MoN. Although further experimental and theoretical studies will be required to obtain a full understanding of the origins of this enhancement, some hypotheses can be put forward by an examination of structural relationship between $Co_{0.6}Mo_{1.4}N_2$ and other Mo-containing HER catalysts. The HER activity observed for MoS_2, Mo_2C, MoB, δ-MoN and Ni−Mo−N suggest that the HER activity in $Co_{0.6}Mo_{1.4}N_2$ originates from surface Mo sites though likely without the severe geometry restrictions of MoS_2 (for which only edge sites are highly active[6]). Given the layered structure, it is expected that catalytically active Mo ions at the surface of $Co_{0.6}Mo_{1.4}N_2$ are coordinated by an interior triangle of three N ligands in a close-packed plane regardless of whether they originate in the trigonal planar or octahedral layers, and that Mo ions have flexibility in their exterior ligands (N^{3-}, NH^{2-}, O^{2-}, OH^-, H^-, H, etc.) whose number and charge may vary during the catalytic cycle. The electronic states of surface Mo species in $Co_{0.6}Mo_{1.4}N_2$ can be tuned by both the strain (smaller *a*-lattice than δ-MoN) and by the chemical bonding originating with the 3d transition metal Co, which may be expected to shift both the position and width of the *d*-electron manifold associated with the surface Mo ions. Since Co ions are readily dissolved under acidic conditions, it is also possible that the activity enhancement is geometric in nature, in which the Co ions in the mixed Co/Mo octahedral layers are removed upon exposure to acid resulting in a large number of highly exposed Mo ions being presented at the catalyst surface. Although synergistic effects due to the presence of both Co and Mo ions at the surface could be postulated, it seems unlikely that this would be responsible for the activity enhancement given the ease with which exposed Co ions can be dissolved in acid. In contrast, Co ions in bulk octahedral layers are protected from acid exposure by Mo ions present within the octahedral layer and by covering Mo ions in neighboring trigonal prismatic layers, allowing good acid stability of bulk Co ions in this electrocatalysis.

Valence and Bonding. Even in the absence of detailed knowledge about the HER reaction mechanism in molybdenum nitrides, it is expected that catalytic activity will be sensitive to the Mo valence and coordination environment. Curiously, a wide range of different bulk Mo valence states are expected for MoS_2 (4+), MoN (3+), MoB (3+), and Mo_2C (2+). The idealized formula of ternary $CoMoN_2$ is expected to correlate with a 4+ valence of Mo that is raised relative to the 3+ valence of binary MoN, though the nonstoichiometric formula of $Co_{0.6}Mo_{1.4}N_2$ indicates a more complex situation. The composition of $Co_{0.6}Mo_{1.4}N_2$ corresponds to an average Mo valence of +3.4 if all Co is divalent, though the presence of cation vacancies in the structure will result in more oxidized Mo ions.

While a bond valence sum (BVS) analysis is often used to gain quantitative insights into the valence of oxides, it is difficult to apply this methodology to the present system since there are not enough close structural analogues with well-defined valence states and well-characterized structures to construct an accurate parametrization. However, meaningful insights into the Mo valence can still be obtained by comparing the Mo−N bond distances in the octahedral (2.17 Å) and trigonal prismatic (2.11 Å) sites of $Co_{0.6}Mo_{1.4}N_2$ to those in reference nitride compounds which also have 6-coordinate Mo (Table S6, Supporting Information). MoN is an appropriate reference for 3+ Mo, and has been reported to have Mo−N bond distances of 2.16 − 2.17 Å in δ-MoN. Similar distances were reported for δ_2 and δ_3 polytypes.[16] These distances are in very good agreement with the sum of the Shannon ionic radii Mo^{3+} and N^{3-} with appropriate coordination number.[21] The octahedral sites in $Co_{0.6}Mo_{1.4}N_2$ can therefore be assigned a valence of 3+, while the trigonal prismatic sites must be higher in valence to account for their reduced Mo−N bond lengths.

The smaller trigonal prismatic average Mo−N bond length (0.06 Å shorter than the octahedral site) in $Co_{0.6}Mo_{1.4}N_2$ suggests a higher valence for this site. The Shannon ionic

dx.doi.org/10.1021/ja4081056 | J. Am. Chem. Soc. 2013, 135, 19186−19192

radii suggest a decrease in ionic radius of 0.04 Å on moving from Mo^{3+} to Mo^{4+}, though it should be noted that the ionic radii of these ions were assigned based on a limited data set (two halide structures for 3+, one halide structure for 4+). Based on its bond length (2.11 Å), the Mo valence on the trigonal prismatic site of $Co_{0.6}Mo_{1.4}N_2$ should be similar to that observed for $MnMoN_2$ (2.12 Å Mo−N bond length) and $Fe_{0.8}Mo_{1.2}N_2$ (2.13 Å) and is probably near 4+ based on these analogies.[19,22] This is larger than the +3.6 valence of the trigonal prismatic site calculated for the $Co_{0.6}Mo_{1.4}N_2$ stoichiometry obtained (assuming that the octahedral site is a mixture of divalent Co and trivalent Mo), though this valence could be raised all the way to +4 if there are ∼20% vacancies on the octahedral cation site. The compound $LiMoN_2$ is expected to have a 5+ Mo valence, and has been reported to have Mo−N a bond length of 2.09 Å[23] which is substantially shorter than observed for $Co_{0.6}Mo_{1.4}N_2$. An analysis of crystal field levels (Figure.5) suggests that Mo^{4+} (d^2) can benefit from the

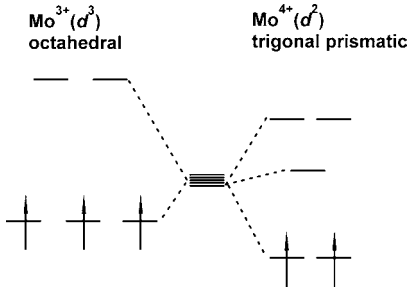

Figure 5. Mo^{3+} (d^3) configuration of an octahedral site (left) and Mo^{4+} (d^2) configuration in a trigonal prismatic site (right), both of which represent the preferred geometry for their indicated oxidation state.

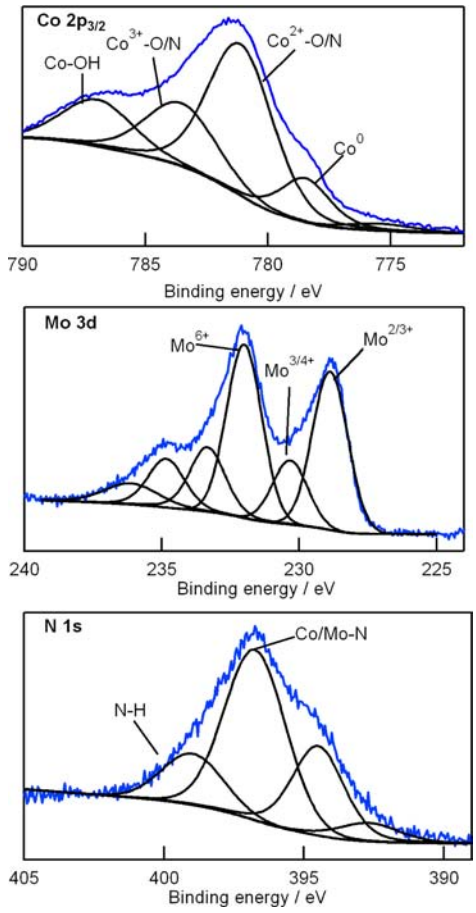

Figure 6. XPS spectra of $Co_{0.6}Mo_{1.4}N_2$: Co 2p, Mo 3d, and N 1s.

distortions associated with a trigonal prismatic environment while Mo^{3+} (d^3) cannot, and that the observed structure of $Co_{0.6}Mo_{1.4}N_2$ does an excellent job of satisfying the bonding preferences associated with the partial oxidation of Mo^{3+}. Similar bonding factors presumably drive the conversion of trigonal prismatic 2H-MoS_2 to octahedral 1T-Li_xMoS_2 (and the accompanying increase in catalytic activity) during the reductive intercalation of Li. In contrast to octahedral 1T-MoS_2 (which was found to transform back to 2H-MoS_2 over a period of weeks[12]), the charge balance in $Co_{0.6}Mo_{1.4}N_2$ is provided by a divalent ion that should be fully immobilized at room temperature allowing the trivalent octahedral Mo^{3+} that is presumably responsible for the enhanced HER activity to be very effectively stabilized.

Further insights into the valence of transition metals at the $Co_{0.6}Mo_{1.4}N_2$ catalyst surface were obtained through XPS measurements (Figure 6). Although Co species may not be directly involved in the HER reaction mechanism, knowledge of the Co valence will be helpful in understanding the Mo valence through charge balance arguments, and the results of the XPS are summarized in Table S7 (Supporting Information). Surprisingly, the composition determined from the XPS analysis (Table S8, Supporting Information) suggests that the sample surface is enriched in Co relative to Mo (1.8:1 Co:Mo ratio, vs 1:1 ratio of starting materials in synthesis). The dominant peak (49%) in the Co $2p_{3/2}$ XPS spectrum at 781.1 eV is from Co^{2+} coordinated to O or N ions, and is attributed to the $Co_{0.6}Mo_{1.4}N_2$ phase. The impurity phase of metallic Co can be seen at 778.5 eV (12%) and the Co^{3+}−O/N bonds which appear at 784 eV (22%) are probably due to the surface oxidation of metallic Co. The remainder of the contribution from the Co metal phase is observed at 787 eV (17%), associated with Co−OH moieties resulting from the reaction of Co metal (or even oxides) with moisture in air.[24] The assignment of a bulk Co valence of 2+ in $Co_{0.6}Mo_{1.4}N_2$ catalyst is supported by this XPS data despite the small amount of observed Co^{3+}, which is believed to only occur through surface oxidation.

The analysis of the $Co_{0.6}Mo_{1.4}N_2$ Mo 3d XPS spectra is more complex due to a spin−orbit coupling feature that splits the 3d response into separate $3d_{5/2}$ and $3d_{3/2}$ peaks. MoO_3 was used as a reference to determine the separation and relative intensities of Mo $3d_{5/2}$ and $3d_{3/2}$ peaks. Fitting of the $Co_{0.6}Mo_{1.4}N_2$ data reveals three Mo $3d_{5/2}$ species: $Mo^{2/3+}$ (229 eV, 55%), $Mo^{3/4+}$ (230 eV, 22%), and Mo^{6+} (232 eV, 22%). In the context of the analysis of bond distances, the first peak is ascribed to Mo^{3+}, the second peak is assigned to Mo^{4+} in the prismatic layer, and the final peak of Mo^{6+} is attributed to surface Mo species that have been oxidized upon air exposure. There is clearly strong ionic character in $Co_{0.6}Mo_{1.4}N_2$, unlike the precursor compound Co_3Mo_3N which exhibits a substantial fraction of Mo^0 and Co^0 character in its XPS spectra (Table S7, Supporting Information). The observed mixture of valence states in $Co_{0.6}Mo_{1.4}N_2$ suggests that the HER electrocatalysis is associated with either the 3+/4+ or 4+/6+ pairs of valence states.

Understanding N 1s XPS peaks is important for nitride compounds, but can only be accomplished after accounting for

dx.doi.org/10.1021/ja4081056 | J. Am. Chem. Soc. 2013, 135, 19186−19192

the effects of partially overlapping Mo $3p_{3/2}$ peaks. This allows two N 1s peaks to be resolved. The major species is N−Co/Mo (397 eV, 84%) which confirms that the surface of $Co_{0.6}Mo_{1.4}N_2$ remains a nitride even after air exposure. This is consistent with the composition calculated by analyzing peak areas (Table S7, Supporting Information), which suggests that the majority of anions at the surface are nitrogens. The N−Co/Mo binding energy is closer to the value expected for Mo−N bonds (396.7 eV) than for Co−N bonds (398.1 eV).[18] The other visible N 1s species is assigned to NH groups (399 eV, 17%) which demonstrates that H species are abundant at the sample surface. Although the origin of the surface H is likely due to an adventitious process such as incomplete reaction with NH_3 or reaction with moisture, this signal does indicate that N ions at the sample surface are able to strongly interact with H species, and that a large number of N−H moieties should be available to participate in the HER reaction mechanism if a reaction pathway of this type is energetically favorable.

CONCLUSIONS

A synthetic route for producing a highly active nanostructured $Co_{0.6}Mo_{1.4}N_2$ non-noble metal electrocatalyst for HER has been demonstrated. This electrocatalyst is shown by neutron diffraction to have a four-layered mixed closed packed structure with alternating layers of octahedral sites (occupied by divalent Co and trivalent Mo) and trigonal prismatic sites (occupied by Mo with a valence larger than three but not more than four), and has not previously been reported to exhibit HER activity. It is expected that the layered nature of this structure allows the 3d transition metal to tune the electronic states of molybdenum at the catalyst surface without disrupting the catalytic activity and that alternative substitutions on the octahedral site of this structure type may lead to even better HER activity. It is desirable to further develop synthetic routes that give more control over particle size and/or access different Mo oxidation states in order to achieve optimal catalytic activity in this structure type and to gain additional experimental and theoretical insights into the mechanism of HER activity in this structure type.

ASSOCIATED CONTENT

Supporting Information

Extended characterization results, including crystal structure analysis, electrochemical data, and XPS data. This material is available free of charge via the Internet at http://pubs.acs.org.

AUTHOR INFORMATION

Corresponding Author

kpete@bnl.gov

Author Contributions

The manuscript was written through contributions of all authors.

Notes

The authors declare no competing financial interest.

ACKNOWLEDGMENTS

This work was carried out at BNL under Contract No. DEAC02-98CH10886 with the U.S. Department of Energy, both in the Chemistry Department and in the Center for Functional Nanomaterials user facility. Primary funding was provided by BNL LDRD 10-0012 (P.G.K., R.R.A.). Acknowledgment is made to the Donors of the American Chemical Society Petroleum Research Fund for partial support of this research (P.G.K.). Research conducted at ORNL's Spallation Neutron Source was sponsored by the Scientific User Facilities Division, Office of Basic Energy Sciences, US Department of Energy. Use of the Advanced Photon Source at Argonne National Laboratory was supported by the U.S. Department of Energy, Office of Science, Office of Basic Energy Sciences, under Contract No. DE-AC02-06CH11357. The research was partially supported by the U.S. Department of Energy, Basic Energy Sciences, Materials Sciences and Engineering Division (G.M.V.). We thank Y. Zhang and J. Wang (BNL) for assistance with caron paper measurements and insightful discussions.

REFERENCES

(1) Walter, M. G.; Warren, E. L.; McKone, J. R.; Boettcher, S. W.; Mi, Q.; Santori, E. A.; Lewis, N. S. *Chem. Rev.* **2010**, *110*, 6446.

(2) Lewis, N. S.; Nocera, D. G. *Proc. Natl. Acad. Sci. U.S.A* **2006**, *103*, 15729.

(3) Holladay, J. D.; Hu, J.; King, D. L.; Wang, Y. *Catal. Today* **2009**, *139*, 244.

(4) Subbaraman, R.; Tripkovic, D.; Strmcnik, D.; Chang, K.-C.; Uchimura, M.; Paulikas, A. P.; Stamenkovic, V.; Markovic, N. M. *Science* **2011**, *334*, 1256.

(5) McKone, J. R.; Sadtler, B. F.; Werlang, C. A.; Lewis, N. S.; Gray, H. B. *ACS Catal.* **2012**, *3*, 166.

(6) Chen, Z.; Cummins, D.; Reinecke, B. N.; Clark, E.; Sunkara, M. K.; Jaramillo, T. F. *Nano Lett.* **2011**, *11*, 4168.

(7) Kong, D.; Wang, H.; Cha, J. J.; Pasta, M.; Koski, K. J.; Yao, J.; Cui, Y. *Nano Lett.* **2013**, *13*, 1341.

(8) Vrubel, H.; Hu, X. *Angew. Chem. Int. Ed* **2012**, *51*, 12703.

(9) Chen, W.-F.; Sasaki, K.; Ma, C.; Frenkel, A. I.; Marinkovic, N.; Muckerman, J. T.; Zhu, Y.; Adzic, R. R. *Angew. Chem. Int. Ed* **2012**, *51*, 6131.

(10) Chen, W.-F.; Wang, C. H.; Sasaki, K.; Marinkovic, N.; Muckerman, J. T.; Zhu, Y.; Adzic, R. R. *Energy Environ. Sci.* **2013**, *6*, 943.

(11) Popczun, E. J.; McKone, J. R.; Read, C. G.; Biacchi, A. J.; Wiltrout, A. M.; Lewis, N. S.; Schaak, R. E. *J. Am. Chem. Soc.* **2013**, *135*, 9267.

(12) Lukowski, M. A.; Daniel, A. S.; Meng, F.; Forticaux, A.; Li, L.; Jin, S. *J. Am. Chem. Soc.* **2013**, *135*, 10274.

(13) Stamenkovic, V. R.; Mun, B. S.; Arenz, M.; Mayrhofer, K. J. J.; Lucas, C. A.; Wang, G.; Ross, P. N.; Markovic, N. M. *Nat. Mater.* **2007**, *6*, 241.

(14) Ham, D. J.; Lee, J. S. *Energies* **2009**, *2*, 873.

(15) Bhattacharyya, S.; Kurian, S.; Shivaprasad, S. M.; Gajbhiye, N. S. *J. Nanopart. Res.* **2010**, *12*, 1107.

(16) Ganin, A. Y.; Kienle, L.; Vajenine, G. V. *J. Solid State Chem.* **2006**, *179*, 2339.

(17) Cao, B.; Veith, G. M.; Diaz, R. E.; Liu, J.; Stach, E. A.; Adzic, R. R.; Khalifah, P. G. *Angew. Chem. Int. Ed* **2013**, DOI: 10.1002/anie.201303197.

(18) Hada, K.; Nagai, M.; Omi, S. *J. Phys. Chem. B* **2001**, *105*, 4084.

(19) Bem, D. S.; Olsen, H. P.; zur Loye, H.-C. *Chem. Mater.* **1995**, *7*, 1824.

(20) Inoue, H.; Wang, J. X.; Sasaki, K.; Adzic, R. R. *J. Electroanal. Chem.* **2003**, *554−555*, 77.

(21) Shannon, R. *Acta Crystallogr., Sect. A* **1976**, *A32*, 751.

(22) Bem, D. S.; Lampe-Onnerud, C. M.; Olsen, H. P.; zur Loye, H.-C. *Inorg. Chem.* **1996**, *35*, 581.

(23) Elder, S. H.; Doerrer, L. H.; DiSalvo, F. J.; Parise, J. B.; Guyomard, D.; Tarascon, J. M. *Chem. Mater.* **1992**, *4*, 928.

(24) McIntyre, N. S.; Cook, M. G. *Anal. Chem.* **1975**, *47*, 2208.